

The published version of the paper " W. Yang, E. Fortunati, F. Dominici, J. M. Kenny, D. Puglia* (2015). Effect of processing conditions and lignin content on thermal, mechanical and degradative behavior of lignin nanoparticles/poly(lactic acid) bionanocomposites prepared by melt extrusion and solvent casting, European Polymer Journal, 71, 126-139" is available at: <https://doi.org/10.1016/j.eurpolymj.2015.07.051>

Effect of processing conditions and lignin content on thermal, mechanical and degradative behavior of lignin nanoparticles/poly(lactic acid) bionanocomposites prepared by melt extrusion and solvent casting

W. Yang, E. Fortunati, F. Dominici, J. M. Kenny, D. Puglia*

*University of Perugia, Civil and Environmental Engineering Department
Materials Engineering Center, UdR INSTM, Terni – Italy*

Abstract

Poly(lactic acid) bionanocomposites filled with 0, 1 and 3 wt. % of lignin nanoparticles (LNPs) were produced by means of two processing techniques, melt extrusion (E-PLA) and solvent casting (C-PLA). The samples were thermally and mechanically characterized by means of thermal analyses (TGA and DSC) and tensile tests. Nucleation effect was proved to be remarkably enhanced when homogeneous dispersion of LNPs in PLA matrix was achieved at 1 wt. %, in melt extruded samples, while further increase of the loading of LNPs up to 3 wt. % did not favor the crystallization behavior. Elongation at break in the case of extruded bionanocomposites was positively affected by the presence of LNPs; nonetheless, in the case of solvent cast films, a decreased tendency of tensile parameters was observed, attributed to inhomogeneous dispersion of LNPs. Disintegrability in composting conditions has been also tested and visual observation, chemical, thermal and morphological investigations proved that the incorporation of 1 wt. % of LNPs seems to hinder the disintegration of PLA matrix, due to the hydrophobic nature of the filler; when the nanoparticles content rise up to 3 wt. %, aggregation and rougher film surface structure induced higher degradation rate.

Keyword: poly (lactic acid), lignin nanoparticles, bionanocomposites, melt extrusion, solvent casting

*Corresponding author: debora.puglia@unipg.it, Tel +390744492916; Fax +390744492950

1. Introduction

The development of synthetic polymers using monomers from natural resources provides a new direction to develop biodegradable polymers from renewable resources. One of the most promising polymers in this regard is Poly (lactic acid) (PLA), because it is made from agricultural products and is readily biodegradable [1-6]. It appears to be one of the most attractive material for applications in agriculture and food packaging sectors, due to its facile availability, good biodegradability and good mechanical properties [7]. Its weaknesses include poor gas barrier properties, low toughness and ductility, poor thermal stability and high cost, so that many research studies have focused on overcoming these limitations, to increase its potential in the fabrication of attractive materials for wide industrial applications [8, 9]. The addition of nanoparticles, as polymer additives, is a very promising approach to improve mechanical properties, elevate heat distortion temperature and enhance barrier properties with an addition of limited amounts of nanofillers (2-8 wt. %) [10].

Like other petrochemical-based plastics, PLA can be processed by various procedures such as injection molding, sheet extrusion, blow molding, and thermoforming [11]. In some previous studies about the use of extruded PLA in combination with cellulose nanocrystals or nanoclays [12-14], a twin-screw extruder was employed to obtain better dispersion of filler particles, providing sufficient dispersive mixing to break up the additive agglomerates. However, this process method has also some detrimental effects, especially for those bio-fillers derived from renewable resources (e.g., natural fibers, starches, proteins, celluloses) due to the unavoidable degradation of the bio-based reinforcements at high processing temperatures. The other processing alternative is the solvent casting technique, in which chloroform, dichloromethane, toluene or a mixture of these three solvents were typically used to dissolve PLA matrix. A good dispersion of nanofillers in PLA matrix could be also achieved after the modification or pretreatment to the nanofillers. In the case of cellulose nanocrystals (CNC), the functionalization with an acid phosphate ester of ethoxylated nonylphenol showed that homogeneous particle dispersion in the polymer matrix did not affect the original PLA transparency. The modified CNC could also induce PLA crystallization, giving a clear enhancement of barrier properties to oxygen and water vapor [10, 15]. Results from organically modified clay/PLA cast solutions also showed that the water vapor barrier property was improved effectively [16]. However, this processing method has a weakness, since agglomeration of these nanofillers can easily form during the film drying step due to their strong propensity to

self-aggregation [17].

Lignin, as the second most abundant renewable and biodegradable natural resource next to cellulose, it is a highly-branched, three dimensional biopolymer. It is a complex macromolecule, based on the repetition of three different phenylpropane units, linked together by ether or C-C bonds. Many functional groups (carbonyl, phenolic or aliphatic hydroxyls, carboxyl etc.) can be found in different proportions of lignin, and the molecular weight can extend from thousand to several tens of thousands [18-21]. The abundance of functional groups on its surface is one of the reasons why it is widely studied as reinforcing filler for plastics and rubber. Recent studies on the use of lignin in composites of thermosets, thermoplastics, elastomers, and foamed materials have been well discussed by Thakur et al. [22]. However, large particle size is a responsible factor against more widespread usage of lignin as filler [23], since the commercial lignin shows particle sizes ranging from 10 μm to even more than 100 μm . Such particles are too large and may exhibit detrimental impacts on mechanical properties of the resulting composites containing the microfiller at variable contents. The reinforcing effect of lignin for polymer matrix intensively depends on particle size and strong interfacial bonding with the matrix.

The aim of this work was to study the effects of different processing methods (melt extrusion via a micro-extruder and solvent casting) on the mechanical and thermal properties of resulted PLA based bionanocomposites reinforced with lignin nanoparticles at two different weight contents (1 wt. % and 3 wt. %), derived from pristine by-product of biomass conversion to bioethanol. In details, morphology, crystallization behavior, mechanical as well as thermal degradative behavior of the extruded and cast neat PLA and PLA/lignin bionanocomposites have been evaluated as a function of composition. In the meanwhile, we focus on analyzing the effects of processing methods on disintegrability in composting conditions of PLA based bionanocomposites.

2. Experimental

2.1 Materials

Poly(lactic acid) (PLA 3251D), with a specific gravity of 1.24 g/cm^3 , a relative viscosity of ca. 2.5, and a melt flow index (*MFI*) of 35 $\text{g}/10$ min (190 $^{\circ}\text{C}$, 2.16 kg) was supplied by Nature Works LLC, USA. PLA pellets were dried in an oven at 40 $^{\circ}\text{C}$ for overnight. Pristine lignin, obtained as bio-residue of conversion of *Arundo donax* L. biomass to bioethanol in a steam explosion pretreatment, followed by enzymatic reactions and filtration, was supplied by CRB (Centro Ricerca

Biomasse, University of Perugia) [24]. Chloroform and all the chemicals were supplied by Sigma-Aldrich.

Lignin nanoparticles (LNPs) synthesis: LNP suspension was prepared from lignin by hydrochloric acidolysis referring to the methods used by Frangville [25] and Gilca [6]. The simplified procedures have been presented in our previous study [27]. **Figure 1a** shows a FESEM image of the obtained cluster structured lignin nanoparticles: size distribution analysis revealed that, after the acidolysis, the typical diameter of the lignin nanoparticles was mainly in the range from 40 to 60 nanometers, no size below 20 or above 80 nm was observed and the average diameter was calculated as 48.9 ± 16.4 nm. The dispersion was frozen for overnight and then moved to freeze dryer (Virtis B.T. 2K ES). Finally, the freeze-dried powder was stored in dry conditions.

2.2 PLA bionanocomposite processing

PLA and PLA nanocomposite films filled with various content of LNP were manufactured by using a twin-screw microextruder and solvent casting methods.

Melt extrusion: neat PLA pellets were introduced into the microextruder and the following parameters were adopted to process the material: screw speed of 100 rpm, a temperature profile of 165-175-180 °C, mixing time of 8 min. LNPs were fed into the microextruder after 2 minutes to limit their thermal degradation. Conditions of a kneading temperature of 180-195-210 °C and a die temperature of 200 °C were selected, in order to obtain PLA and PLA bionanocomposite films with a thickness ranged from 20 to 40 µm. The materials have been designed as E-PLA, E-PLA/1LNP and E-PLA/3LNP, indicating the PLA bionanocomposites prepared by extrusion containing 0, 1 or 3 wt. % of LNPs, respectively.

Solvent casting: neat PLA (2 g) was dissolved in 20 mL of chloroform with vigorous stirring at room temperature (RT). LNPs were added after complete dissolution of PLA. The solutions were stirred for another 2 h, after that a treatment of sonication (Vibracell, 750) for 2 min in an ice bath was performed, in order to improve the LNP dispersion in chloroform. The solutions were then cast onto a 15 cm diameter glass Petri dish, and then allowed to dry for about 24 h at RT. The resultant films with a thickness of ca. 80-100 µm were peeled from the Petri dish after drying. The solvent cast films were placed in a vacuum oven at 40 °C for 1 week in order to remove all remaining chloroform. The obtained films have been designed as C-PLA, C-PLA/1LNP and C-PLA/3LNP, representing the materials prepared by solvent casting containing 0, 1 or 3 wt. % of LNPs,

respectively.

2.3 PLA bionanocomposite characterization

2.3.1 Differential scanning calorimeter (DSC)

DSC (TA Instrument, Q200) measurements were performed in the temperature range from -25 to 210°C at 10 °C/min under nitrogen flow. PLA and PLA nanocomposite samples (6–8 mg) were heated from -25 to 210 °C at a heating rate of 10°C/min and held at 210°C for 2 min to eliminate the thermal history (1st heating scan), then they were cooled to -25 at 10°C/min and reheated under the same conditions (2nd heating scan). Glass transition, cold crystallization and melting temperatures (T_g , T_{cc} and T_m), such as ΔH_{cc} and ΔH_m , were determined from the second heating scans. The crystallinity degree (χ) was calculated from the second scan as reported in Equation (1):

$$\chi = \frac{\Delta H_m - \Delta H_{cc}}{\Delta H_{m0} (1 - m_f)} \times 100 \quad (1)$$

where ΔH_m and ΔH_{cc} are the enthalpies of melting and cold crystallization, respectively, ΔH_{m0} is enthalpy of melting for a 100% crystalline PLA sample, taken as 93 J/g [28] and $(1 - m_f)$ is the weight fraction of PLA in the sample.

2.3.2 Thermogravimetric analysis (TGA)

TGA tests were carried out by using a Thermo gravimetric Analyzer (TGA, Seiko Exstar 6300). The samples, approximately 8 mg, were heated from 30 to 800 °C at a heating rate of 10 °C/min under nitrogen atmosphere. The weight-loss rate was obtained from derivative thermogravimetric (DTG) data. The onset degradation temperature (T_{onset}) was defined as the 1% weight loss drawn from the TG curves after 200 °C at which the samples begin to degrade. Temperatures of maximum degradation rate (T_{max}) were also collected from maxima of DTG peaks, along with the residual weight percent measured at 600 °C.

2.3.3 Mechanical behavior

The mechanical performance of neat PLA and PLA bionanocomposite systems was evaluated by means of tensile tests, performed on rectangular probes (100 mm x 10 mm) on the basis of UNI ISO 527 standard with a crosshead speed of 5 mm/min, a load cell of 500 N and an initial gauge length of 25 mm. Average tensile strength (σ), elastic modulus (E) and elongation at break (ϵ_b) were

calculated from the resulting stress-strain curves. The measurements were done at room temperature and at least five samples were tested for each formulation.

2.3.4 Morphology

The microstructure of PLA bionanocomposite films was investigated by a field emission scanning electron microscope (FESEM, Supra 25-Zeiss, Germany). The fractured surfaces of the samples, obtained by liquid nitrogen, were observed after gold sputtering.

2.4 Disintegrability in composting conditions

Disintegrability of cast or extruded PLA and PLA bionanocomposites films was evaluated by means of a disintegration test in composting conditions according to the ISO-20200 standard. A specific quantity of compost, supplied by Gesenu S.p.a. (Italy), was mixed together with the synthetic biowaste, prepared with certain amount of sawdust, rabbit food, starch, sugar, oil and urea. The water content of the substrate was around 50 wt. % and the aerobic conditions were guaranteed by mixing it softly. The samples were buried at 4–6 cm depth in perforated boxes, containing the prepared mix, and incubated at 58 °C. The (15 mm x 15 mm) films were recovered at different disintegration steps, washed with distilled water, dried in oven at 37 °C for 24 h, and weighed. The disintegrability value was obtained normalizing the sample weight, at different stages of incubation, to the initial ones. In order to better discuss the results of disintegration experiment, water contact angle measurements of all materials were performed by using a FTA1000 Analyzer. Surface microstructure of the composites before the composting and at different days of incubation was investigated by FESEM, while sample photographs were taken for visual comparison. DSC analysis of samples at different disintegration times was performed under nitrogen flow condition, from -25 to 210 °C at a heating rate of 10 °C/min. Fourier infrared spectra of the degraded samples were recorded by a Jasco FT-IR 615 spectrometer, in attenuated total reflection (ATR) mode, in the 400–4000 cm⁻¹ range.

3. Results and discussion

3.1 Differential scanning calorimeter (DSC)

DSC analysis was used to investigate the glass transition (T_g), cold crystallization (T_{cc}), melting

temperatures (T_m) and crystallinity (X_c) of PLA and PLA nanocomposites. Thermograms for all the different materials related to the first heating scan, cooling and second heating scan are shown in **Figure 1b**, **Figure 1c** and **Figure 1d**, respectively. Calorimetric parameters from first heating and second heating scans for all materials are also reported in **Table 1 (a and b)**. The analysis of the heat flow curves at the first heating scan confirmed that limited variations were observed for the main melting event for samples obtained with the two different techniques, while an additional exothermic peak (a shoulder crystallization peak) that occurs prior to the major melting peak was observed in the case of extruded PLA bionanocomposites. A small melt recrystallization exotherm preceding the main melting endotherm of PLA appears, due to rapid cooling, already reported in He et al. [29, 30]. The measured values of T_g in the case of cast systems, at first heating scan, were lower than glass transition temperatures of extruded samples, due to the presence of residual solvent. The glass transition temperature of extruded PLA films containing 1% wt. of LNPs was slightly lower than the one of the neat PLA, and this may be attributed to a plasticizing effect of a low molecular weight fraction of lignin [31]. When increased amount of lignin was added to PLA, the cold crystallization temperature shifted to lower temperatures in the case of extruded material (from the original 101.7°C to 100.8°C and 96.1°C for E-PLA/1LNP and E-PLA/3LNP, respectively). In the case of cast samples, the segmental motion of PLA molecular chains ($T_{cc}=94.2^\circ\text{C}$) may have been affected by presence of lignin, leading to a shift in the T_{cc} to higher temperatures (mean values of 94.9°C and 95.5°C for C-PLA/1LNP and C-PLA/3LNP, respectively) [32].

In the cooling scans (**Figure 1c**), exothermic peaks with very low intensity were observed for the solvent cast bionanocomposite samples, indicating a rather low crystallization capability [33]. These three samples did not allow the observation of crystallization temperature (T_c). In the case of melting extruded bionanocomposite samples, the adding of LNP gradually increased the T_c from 91.2 to 97.1 °C, the crystallization peaks had relatively higher intensity as a result of enhanced crystallization ability, in which E-PLA/1LNP exhibited the highest intensity of exothermic peak. The nucleation effect was remarkably enhanced when homogeneous LNP dispersion in PLA matrix was achieved, by using melt extrusion processing method. This effect is evidenced in the crystallinity values registered in the 2nd heating scan (**Table 1b**). For the solvent cast films, the addition of LNP has no influence on the crystallization of the resulted PLA matrix, since no significant increase in crystallinity could be observed in these cases. On the contrary, a remarkable

increase of crystallinity was obtained for the PLA filled with 1 wt. % of LNPs from 15.0 ± 1.0 to $22.5 \pm 1.4\%$ (prepared by melt extrusion), implying an homogeneous dispersion of LNP fillers in PLA. However, a further increase of the loading of LNPs up to 3 wt. % (E-PLA/3LNP) did not favor the crystallization behavior of PLA matrix, as only $17.4 \pm 1.1\%$ of crystallinity, a slight increase compared with E-PLA, was achieved. The reason for this result was not clear, maybe LNP fillers aggregated during the preparation of the films, or the LNP fillers served as toughness agents instead of nucleating among the PLA polymer chains [34]. After eliminating the thermal history, similar curves were observed for extruded and solvent cast samples in the second heating scan, indicating the same crystallization behaviors and phases. However, a relative higher T_{cc} could be also observed in the cases of cast films when comparing with melting extruded films, confirming a low crystallization capability.

3.2 Thermogravimetric analysis (TGA)

The weight-loss curves as a function of the temperature are shown in **Figure 2**. Thermal stability test results for the PLA films are also shown in **Table 2**. The solvent cast PLA films decreased about 10% with respect to their initial weight during heating between 80 and 150°C because of the removal of the residual solvent in the films [29]. In the extruded films, an increase for T_{onset} with increasing LNP loading was observed, as T_{onset} of neat E-PLA was 259.0 °C, while 263.7 and 274.7 °C were measured for E-PLA/1LNP and E-PLA/3LNP, respectively, indicating that LNP will improve the heat resistance of resulted bionanocomposite films. Moreover, the residual weight (char yield) obtained at 900 °C also gradually increased from 0.02 % for E-PLA up to 1.08 and 2.23 % for E-PLA/1LNP and E-PLA/3LNP, respectively, due to the chemical structure of lignin, which was demonstrated to weakly contribute to material flammability due to a high charring ability and a low heat release when burning [30]. These positive results could be attributed to the homogeneous dispersion of LNP in the PLA matrix by using a melt extrusion processing method. It should be noted that the introduction of LNP does not increase the T_{max} , and this may be due to the same range of degradation temperature of LNP with respect to PLA, as reported in our previous study [27]. However, in the solvent cast films, the increasing loading of LNP did not influence the T_{onset} , even an opposite tendency for residual weight of the resulted materials was detected when compared with the melting extruded films. This was supposed to be due to the strong tendency of self-aggregation

of this nano-phase fillers during the film drying phase [17].

3.3 Tensile properties

The tensile properties of the films are very important in selecting diverse applications for polymeric formulations. Parameters as tensile strength (σ), modulus (E), and elongation at break (ϵ_b) indicate the ability of films to maintain integrity under the stress occurring during the processing, handling, and storage of the packaged materials [35]. **Figure 3a-c** showed the results of tensile test in terms of strength, modulus and elongation at break, while the typical stress-strain curves for all studied materials are reported in **Figure 3d**. The PLA film without LNP (C-PLA) prepared by solvent casting method kept the same level of strength and elongation at break but lower modulus (due to the plasticizer effect due to the residual chloroform captured in the films) than the PLA film (E-PLA) prepared by the melt extrusion method. The introduction of 1 wt. % of LNP (E-PLA/1LNP) increased the σ and E from 44.3 and 1955.8 MPa to 48.7 and 2153.2 MPa, respectively. Furthermore, ϵ_b for E-PLA/1LNP also reached 26.7 % when compared with E-PLA (16.8 %), which was contradictory with many nanocomposites bearing rigid nanofillers. This result was supposed to be related to the special chemical structure of lignin, bearing a lot of functional groups (carbonyl, phenolic or aliphatic hydroxyls, carboxyl), which intensively contributed to the interactions (like hydrogen bonding) between PLA matrix and LNP [36, 37]. When the loading of LNP increased to 3 wt. % (E-PLA/3LNP), the ϵ_b further increased to 66.2 %, with a reduction of σ (41.0 MPa) and E (1390.6 MPa) with respect of E-PLA. Our experimental results in terms of reduction of tensile strength and tensile modulus are in line with previous studies of PLA-lignin blends, which showed a reduction in the tensile strength with the increase of lignin loading. This behavior was explained considering that the decrease in the mechanical properties was due to the existence of lignin particles which prevented the formation of a long range continuous phase of PLA [38]. Indeed, it has been already observed [34] that enhanced elongation at break of neat PLA in presence of lignin particles can be attributed to the flexibility of the lignin structure (benzene rings are linked with ether linkages that act as internal plasticizers [39-40]). These previous studies were related to the use of lignin microparticles in PLA and it supposed that the mechanism is still valid even in the presence of nanosized lignin.

Nonetheless, in the case of solvent cast film, a decreased tendency of σ , E, and ϵ_b was observed, which was supposed to be attributed the inhomogeneous dispersion of LNP and the induced poor

interactions between LNP and PLA matrix. At macro level, the LNP disperse well in the PLA matrix, thus a toughening effect and good interaction between PLA and LNP were achieved, and this effect was revealed in the case of extruded samples. Indeed, at the microscale, some LNP fillers would aggregate during the preparation procedures, especially in the case of casted films.

3.4 Morphology

FESEM images of the fractured surfaces for extruded and solvent cast PLA and PLA bionanocomposite films are shown in **Figure 4**. The surface structure between extruded and casting films exhibited an obvious difference as smoother surface morphology could be observed in the extruded films. In the extruded films, no micro-domains can be observed, the surface resulted homogeneous due to the obtained good distribution of LNP nanofillers in PLA matrix during the process, confirming the improved mechanical performance of the nanocomposites containing lignin nanoparticles at the two different weight amounts. Nevertheless, some micro-domains and many micro-holes can be observed in C-PLA/1LNP and C-PLA/3LNP, and their surface is also less homogeneous than C-PLA. These micro-holes and micro-domains should be related to the evaporation of the chloroform solvent and a phase separation between PLA and lignin, more evident in the sample containing 3 wt. % of LNPs.

3.5 Disintegrability in compost of PLA nanocomposites

The disintegration in composting conditions of PLA is one of the most attractive properties for packaging applications [41]. Its degradation usually starts with the hydrolysis of the PLA chains induced by the diffusion of water into the materials. The effect of nanoparticles addition over PLA degradation in compost has been reported over the past few years. The influence over the degradation process strongly depends on the hydrophilicity/hydrophobicity and dispersion of the nanoparticles. Moreover, a delayed biodegradability due to the improved barrier properties of the nanomaterials was previously observed, which could hinder the water diffusion through the bulk [42]. The study of the disintegration in composting conditions of PLA and PLA bionanocomposites was carried out to evaluate the effect of the addition of LNP and processing methods on the disintegrability properties of the PLA matrix. **Figures 5a** (extruded films) and **Figure 5b** (cast films) shows photographs of all the samples at different composting times up to 29 days. Whitening and

deformation of the film surfaces were detected just after the first day of incubation for all materials and these effects were enhanced after 3 days in composting conditions. These results are indicative of the beginning of the hydrolytic degradation, in which extruded films were faster than casting films when taking into account the thickness difference between them. The loss of transparency observed for all samples could be attributed to changes in the refractive index due to the water absorption and the formation of low molecular weight compounds after the hydrolytic degradation [43, 44]. The color changes are also linked with sample degradation process and embrittlement, leading to their breakage. It has been indicated that the PLA hydrolysis begins in the amorphous region of the polymer structure and all these effects would also result in changes in the polymer crystallinity and consequently in loss of transparency [45]. Moreover, it should be taken into account that the degradation experiments took place at 58 °C, which is the region of glass transition of PLA. This could increase the chain mobility, inducing the crystallization of the PLA matrix.

The disintegrability in composting conditions was also evaluated in terms of mass loss at different incubation times. The disintegration process takes place between 7 and 10 days of incubation for extruded films, and between 7 and 15 days for solvent casting films, as reported in **Figure 6**. The disintegrability value remains constant for all systems until 3 days of incubation, while reaches 30–50% at 10 days for all extruded PLA bionanocomposite films. The incorporation of 1 wt. % of LNP seems to hinder the disintegration of PLA matrix, as a low weight loss can be observed in E-PLA/1LNP for 10 days of incubation, and the same behavior can be detected for C-PLA/1LNP for 15 days of incubation in compost. This behavior could be attributed to the double effect caused by the addition of a hydrophobic nanofiller: LNPs are expected to delay the degradation rate of the PLA bionanocomposites, in the meanwhile the homogeneous dispersion of 1 wt. % of LNP could also limit the water diffusion by the increase of barrier properties and consequently delaying hydrolysis and further degradation [10]. On the other hand, when the LNP content rise up to 3 wt. %, some LNP aggregations and rougher film surface structure could form, inducing higher degradation rate. These results underlined that all the studied bionanocomposites started the disintegration process after and with lower rate than neat PLA films, suggesting their perspective advantages in industrial applications when long biodegradation times are required.

Table 3 showed the water contact angle for the extruded and cast PLA bionanocomposite films. Overall, the contact angle of casting films was lower than extruded ones due to the presence of

some residual polar solvent chloroform in the cast films. It was interesting to observe that the contact angle of E-PLA/1LNP (71.1°) was higher than E-PLA (70.2°). The main reason for the increase in contact angle has to be related to the presence of lignin nanoparticles. Indeed, lignin is known to be a hydrophobic molecule because of its aromatic skeleton and non-polar hydrocarbon chains in the lignin molecules, which naturally reduces the hydrophilicity of the composites [44-48]. Actually, LNP has already been shown to reduce the water sensitivity [27]. However, when the loading of LNP increased to 3 wt. %, the contact angle decreased to 69.8° (E-PLA/3LNP), and the same tendency could be also observed for the cast films. This could be attributed to the formation of some LNP aggregations and rougher film surface structure compared to E-PLA/1LNP or C-PLA/1LNP nanocomposites, which resulted in reducing the contact angle. The results are consistent with the results in term of mass loss obtained in the disintegration experiment.

3.5.1 FTIR analysis of degraded samples

In order to evaluate the extent of disintegration in composting conditions of the different samples, FTIR analysis of materials at the initial state and at different stage of the degradation were carried out. **Figure 7** shows the FTIR spectra of the samples at different incubation times. The infrared spectra of PLA bionanocomposites display the typical stretching of carbonyl group (-C=O-) at 1750 cm^{-1} by lactide, and the -C-O- bond stretching in the -CH-O- group of PLA at 1182 cm^{-1} , while the broad peak appeared at 1040 cm^{-1} (-C-O stretch of polysaccharide) shows the presence of non-decomposed, unstable polysaccharide. The intensities of the -C=O- bands of PLA show sharpening and increase after biodegradation. The changes of -C=O- band are associated with the increase in the number of carboxylic end groups in the polymer chain during the hydrolytic degradation [49,50]. During degradation in the case of E-PLA film (**Figure 7a**), the intensity of the above bands became stronger up to 7 days, indicating a progressive degradation of the PLA matrix. Compared with E-PLA, E-PLA/1LNP (**Figure 7b**) exhibited a weaker intensity of the above bands not only in 3 days but also up to 7 days, illustrating a lower degradation rate and good barrier property of LNP in PLA matrix. For E-PLA/3LNP (**Figure 7c**), the biodegradation rate shows difference with respect to the other two films and some peaks almost disappeared, the relative height of the aromatic region at 1650 cm^{-1} rose as the composting process proceeded and this change in the spectrum indicates that easily degradable organic matter constituents such as short

aliphatic chains, polysaccharides and alcohols are chemically or biologically oxidized, leading to increased aromatic structures of high stability [51, 52]. The FTIR results also demonstrated that the degradation in composting of PLA was mainly caused by microorganism erosion and the erosion originated from the surface layer then spread gradually to the interior of the material, since the chemical structure of residual PLA was not changed during the degradation process. The C-PLA film showed the similar biodegradation process as to E-PLA film in 7 days of incubation time, since the similar spectra are presented in **Figure 7d**. Nevertheless, in the case of C-PLA/1LNP and C-PLA/3LNP films (**Figures 7e** and **7f**) no significant changes occurred after 7 days, since the incorporation of LNP and their preferential barrier property. After 15 days of incubation in compost, all peaks of the three casting films disappeared, demonstrating a deeper degradation process of PLA matrix. The FTIR investigation confirmed the variation of weight loss discussed above.

3.5.2 Thermal analysis of degraded samples

Figure 8 shows the DSC thermograms obtained from the first heating cycle for samples after different disintegration times. The glass transition temperatures (T_g) and melting temperatures (T_m), obtained from analysis of DSC curves at different incubation times are summarized in **Table 4**. The peak of the glass transition temperature gradually disappears, as expected, during disintegration due to moisture absorption with increasing the incubation time in compost, since water could serve as a plasticizer agent in polymer matrix. Moreover, the gradual disintegration of PLA does not allow the observation of cold crystallization at composting times above 3 days, and the melting peaks also gradually disappeared, accompanying with a decreasing T_m for all extruded and casting films. The lower temperature melting peak is ascribed to the melting of less perfect crystals while the high temperature one to the melting of more perfect crystals within the same lamellae [53, 54]. Upon degradation, the presence of an additional melting peak in the case of neat matrix (E-PLA/7d) can be associated to the formation of crystals with a different structure or of less perfect crystals, due to the polymer chains scission during the hydrolytic process, resulting in a decrease of the crystal lamellae thickness and perfection [55, 56].

3.5.3 Surface analysis of degraded samples

Morphological characterization of PLA/lignin based systems after different incubation times was

carried out to evaluate the effect of composting conditions on the material surface morphology. Scanning electron micrographs (**Figure 9a** and **Figure 9b**) show that PLA surface is characterized by regular transverse striations after 7 days of disintegration experiment. These could be generated by the accumulated erosion of the amorphous macromolecules on the surface, giving rise to the deeper grooves. This is quite typical in cases where PLA has not a very high crystallinity, and it is subjected to soil burial, which implies the exposure to a non neutral environment [57]. For extruded films (**Figure 9a**), some LNP aggregations could be seen in E-PLA/1LNP and E-PLA/3LNP, while more and bigger aggregations were shown in E-PLA/3LNP. Furthermore, more cracks were shown in E-PLA/3LNP bionanocomposites. In the meanwhile, a rougher film surface structure could be observed for C-PLA/3LNP bionanocomposite, when compared to C-PLA/1LNP (**Figure 9b**). These results fully support our previous predictions and give the evidences to explain the variation of water contact angle and degradation process in all bionanocomposites.

As a general consideration, the disintegration process is triggered by two main factors, which are the low crystallinity of the PLA matrix used and the percent of LNP used in the formulations: both are well known occurrences in biopolymers [58]. These factors would need to be accurately dealt with in selecting matrix and filler content for possible applications of a fully biodegradable and compostable lignin nanoparticles reinforced PLA composite.

4. Conclusions

Poly(lactic acid) bionanocomposites, filled with 0, 1 and 3 wt. % of LNPs were successfully produced by means of melt extrusion and solvent casting. The nucleation effect was remarkably enhanced when homogeneous dispersion of LNP in PLA matrix was achieved at 1 wt. %, by using melt extrusion processing method. For the solvent cast films containing the same amount of LNPs, the addition of LNPs has no influence on the crystallization of the resulted PLA matrix. Further increase of the loading of LNPs up to 3 wt. % (E-PLA/3LNP) did not favor the crystallization behavior of PLA matrix, since lignin nanoparticles aggregated during the preparation of the films. Mechanical properties, especially the elongation at break in the case of extruded bionanocomposites, was positively affected by the presence of LNPs, and this result was supposed to be related to the chemical nature of lignin. Nonetheless, in the case of solvent cast films, a decreased tendency of σ , E , and ϵ_b was observed, mainly ascribed to the inhomogeneous dispersion of LNP and relatively weak interactions between LNP and PLA matrix. Results of disintegrability tests in composting

conditions proved that the incorporation of 1 wt. % of LNP seems to hinder the disintegration of PLA matrix, due to the hydrophobic nature of the filler. In addition, when the LNP contents rise up to 3 wt. %, LNP aggregation and rougher film surface structures were detected, inducing higher degradation rates. These results underlined that all the studied bionanocomposites started the disintegration process after and with lower rate than neat PLA films, suggesting their perspective advantages in industrial applications when long biodegradation times are required.

Acknowledgements

This research has been developed in the frame of the BIT3G Project - Third generation bio refinery integrated in the territory, financed by the Italian Ministry for Education and Research (MIUR - project: CTN01_00063_49295). Weijun Yang appreciates the funding support of China Scholarship Council (CSC). The Authors acknowledge Gesenu S.p.a. for compost supply.

Figures and Tables captions

Figure 1: FESEM image of lignin nanoparticles, 200 nm scale (a), DSC thermograms of extruded and solvent cast PLA and PLA/LNP bionanocomposites at 1st heating run (b), cooling (c) and 2nd heating run (d).

Figure 2: Residual mass curves and derivative curves vs temperature of extruded and solvent cast PLA and PLA/LNP bionanocomposites.

Figure 3: Values for tensile strength (a), Young's modulus (b), elongation at break (c) and stress-strain curves for extruded and solvent cast PLA and PLA/LNP bionanocomposites.

Figure 4. FESEM images of fractured cross sections for extruded and solvent cast PLA and PLA/LNP bionanocomposites.

Figure 5. Visual observation of PLA and PLA/LNP bionanocomposites before (0 day) and after different stages of disintegration in composting at 58 °C for extruded (a) and cast films (b)

Figure 6. Disintegrability values of extruded and solvent cast PLA and PLA/LNP bionanocomposites at different stages of incubation in composting.

Figure 7. FTIR spectra of extruded (a, b, and c) and solvent cast (e, f and g) PLA and PLA/LNP bionanocomposites after different stages of incubation in composting.

Figure 8. DSC curves (1st heating run) of extruded (a, b, and c) and solvent cast (e, f and g) PLA and PLA/LNP bionanocomposites after different stages of incubation in composting.

Figure 9. FESEM images of extruded (a) and solvent cast PLA and PLA/LNP bionanocomposites (b) after different stages of incubation in composting.

Table 1: T_g (glass transition), T_{cc}(cold crystallization), T_m (melting) temperatures and crystallinity (X_c) measured in the 1st heating (a) and 2nd heating scans (b) for PLA and PLA/LNP bionanocomposites

Table 2. Onset temperatures, maximum degradation rate temperatures and residual mass at 600°C measured for PLA and PLA/LNP bionanocomposites

Table 3: Water contact angles for PLA and PLA/LNP bionanocomposites obtained by melt extrusion and solvent casting

Table 4: T_g (glass transition) and T_m (melting temperatures) measured in the 1st heating scan for PLA and PLA/LNP bionanocomposites at different disintegration times

References

- [1] Processing and characterization of natural cellulose fibers/thermoset polymer composites. *Carbohydrate Polymers*, 109,102-117, 2014;
- [2] Review: Raw Natural Fiber-Based Polymer Composites, *International Journal of Polymer Analysis and Characterization*, 19, 3, 256-271, 2014;
- [3] Recent advances in graft copolymerization and applications of chitosan: a review, *ACS Sustainable Chemistry & Engineering* 2 (12), 2637-2652, 2014;
- [4] Advances in Industrial Prospective of Cellulosic Macromolecules Enriched Banana biofibre resources: A Review, *International Journal of Biological Macromolecules*, 79, 449-458 (2015)
- [5] Recent advances in green hydrogels from lignin: a review, *International journal of biological macromolecules* 72, 834-847 10 (2015)
- [6] Self-healing polymer nanocomposite materials: A review 69, 369-383 (2015).
- [7] Vannier A, Duquesne S, Bourbigot S, Castrovinci A, Camino G, Delobel R. The use of POSS as synergist in intumescent recycled poly (ethylene terephthalate). *Polymer Degradation and Stability*. 2008;93(4):818-826.
- [8] Jamshidian M, Tehrani EA, Imran M, Akhtar MJ, Cleymand F, Desobry S. Structural, mechanical and barrier properties of active PLA–antioxidant films. *Journal of Food Engineering*. 2012;110(3):380-389.
- [9] Jonoobi M, Harun J, Mathew AP, Oksman K. Mechanical properties of cellulose nanofiber (CNF) reinforced polylactic acid (PLA) prepared by twin screw extrusion. *Composites Science and Technology*. 2010;70(12):1742-1747.
- [10] Fortunati E, Rinaldi S, Peltzer M, Bloise N, Visai L, Armentano I, et al. Nano-biocomposite films with modified cellulose nanocrystals and synthesized silver nanoparticles. *Carbohydrate Polymers*. 2014;101(0):1122-1133.
- [11] Lim LT, Auras R, Rubino M. Processing technologies for poly(lactic acid). *Progress in Polymer Science*. 2008;33(8):820-852.
- [12] Fortunati E, Armentano I, Zhou Q, Iannoni A, Saino E, Visai L, et al. Multifunctional bionanocomposite films of poly(lactic acid), cellulose nanocrystals and silver nanoparticles. *Carbohydrate Polymers*. 2012;87(2):1596-1605.
- [13] Fukushima K, Tabuani D, Arena M, Gennari M, Camino G. Effect of clay type and loading on

thermal, mechanical properties and biodegradation of poly (lactic acid) nanocomposites. *Reactive and Functional Polymers*. 2013;73(3):540-549.

[14] Bourbigot S, Duquesne S, Fontaine G, Bellayer S, Turf T, Samyn F. Characterization and reaction to fire of polymer nanocomposites with and without conventional flame retardants. *Molecular Crystals and Liquid Crystals*. 2008;486(1):325/[1367]-1339/[1381].

[15] Fortunati E, Peltzer M, Armentano I, Jiménez A, Kenny JM. Combined effects of cellulose nanocrystals and silver nanoparticles on the barrier and migration properties of PLA nano-biocomposites. *Journal of Food Engineering*. 2013;118(1):117-124.

[16] Rhim J-W, Hong S-I, Ha C-S. Tensile, water vapor barrier and antimicrobial properties of PLA/nanoclay composite films. *LWT - Food Science and Technology*. 2009;42(2):612-617.

[17] Liu D, Zhong T, Chang PR, Li K, Wu Q. Starch composites reinforced by bamboo cellulosic crystals. *Bioresource Technology*. 2010;101(7):2529-2536.

[18] Boeriu CG, Bravo D, Gosselink RJA, van Dam JEG. Characterisation of structure-dependent functional properties of lignin with infrared spectroscopy. *Industrial Crops and Products*. 2004;20(2):205-218.

[19] Baumberger S, Abaecherli A, Fasching M, Gellerstedt G, Gosselink R, Hortling B, et al. Molar mass determination of lignins by size-exclusion chromatography: towards standardisation of the method. *Holzforschung*. 2007;61(4):459-468.

[20] El Mansouri N-E, Salvadó J. Analytical methods for determining functional groups in various technical lignins. *Industrial Crops and Products*. 2007;26(2):116-124.

[21] Wieser H. Chemistry of gluten proteins. *Food microbiology*. 2007;24(2):115-119.

[22] Thakur VK, Thakur MK, Raghavan P, Kessler MR. Progress in green polymer composites from lignin for multifunctional applications: A review. *ACS Sustainable Chemistry & Engineering*. 2014;2(5):1072-1092.

[23] Bahl K, Miyoshi T, Jana SC. Hybrid fillers of lignin and carbon black for lowering of viscoelastic loss in rubber compounds. *Polymer*. 2014;55(16):3825-3835.

[24] Cotana F, Cavalaglio G, Nicolini A, Gelosia M, Coccia V, Petrozzi A, et al. Lignin as co-product of second generation bioethanol production from ligno-cellulosic biomass. *Energy Procedia*. 2014;45:52-60.

[25] Frangville C, Rutkevičius M, Richter AP, Velev OD, Stoyanov SD, Paunov VN. Fabrication of

- Environmentally Biodegradable Lignin Nanoparticles. *ChemPhysChem*. 2012;13(18):4235-4243.
- [26] Gilca IA, Ghitescu RE, Puitel AC, Popa VI. Preparation of lignin nanoparticles by chemical modification. *Iranian Polymer Journal*. 2014;23(5):355-363.
- [27] Yang W, Kenny JM, Puglia D. Structure and properties of biodegradable wheat gluten bionanocomposites containing lignin nanoparticles. *Industrial Crops and Products*. 2015;74(0):348-356.
- [28] Martin O, Avérous L. Poly(lactic acid): plasticization and properties of biodegradable multiphase systems. *Polymer*. 2001;42(14):6209-6219.
- [29] He Y, Wu T, Wei J, Fan Z, Li S. Morphological investigation on melt crystallized polylactide homo-and stereocopolymers by enzymatic degradation with proteinase K. *Journal of Polymer Science Part B: Polymer Physics*. 2008;46(10):959-970.
- [30] Detyothin S, Selke SE, Narayan R, Rubino M, Auras R. Reactive functionalization of poly(lactic acid), PLA: Effects of the reactive modifier, initiator and processing conditions on the final grafted maleic anhydride content and molecular weight of PLA. *Polymer Degradation and Stability*. 2013;98(12):2697-2708.
- [31] Domenek S, Louaifi A, Guinault A, Baumberger S. Potential of lignins as antioxidant additive in active biodegradable packaging materials. *Journal of Polymers and the Environment*. 2013;21(3):692-701.
- [32] Mu C, Xue L, Zhu J, Jiang M, Zhou Z. Mechanical and Thermal Properties of Toughened Poly(L-lactic) Acid and Lignin Blends. *BioResources*. 2014;9(3):5557-5566.
- [33] Pei A, Zhou Q, Berglund LA. Functionalized cellulose nanocrystals as biobased nucleation agents in poly(l-lactide) (PLLA) – Crystallization and mechanical property effects. *Composites Science and Technology*. 2010;70(5):815-821.
- [34] Sun Y, Yang L, Lu X, He C. Biodegradable and renewable poly(lactide)–lignin composites: synthesis, interface and toughening mechanism. *Journal of Materials Chemistry A*. 2015.
- [35] Rhim JW, Mohanty AK, Singh SP, Ng PK. Effect of the processing methods on the performance of polylactide films: thermocompression versus solvent casting. *Journal of Applied Polymer Science*. 2006;101(6):3736-3742.
- [36] Ferry L, Dorez G, Taguet A, Otazaghine B, Lopez-Cuesta J. Chemical modification of lignin by phosphorus molecules to improve the fire behavior of polybutylene succinate. *Polymer*

Degradation and Stability. 2014.

[37] Thunga M, Chen K, Grewell D, Kessler MR. Bio-renewable precursor fibers from lignin/poly lactide blends for conversion to carbon fibers. *Carbon*. 2014;68:159-166.

[38] Ouyang W, Huang Y, Luo H, Wang D. Poly(Lactic Acid) Blended with Cellulolytic Enzyme Lignin: Mechanical and Thermal Properties and Morphology Evaluation *J. Polym. Environ* 20 (2012) 1-9.

[39] Wang K, Bauer S, Sun R. Structural transformation of *Miscanthus × giganteus* lignin fractionated under mild formosolv, basic organosolv, and cellulolytic enzyme conditions *J Agric Food Chem*, 60 (2012) 144–152.

[40] Mu C, Xue L, Zhu J, Jiang M, Zhou Z. Mechanical and Thermal Properties of Toughened. Poly(L-lactic) Acid and Lignin blends. *BioResources* 9(3), (2014) 5557-5566.

[41] Kale G, Auras R, Singh SP, Narayan R. Biodegradability of polylactide bottles in real and simulated composting conditions. *Polymer Testing*. 2007;26(8):1049-1061.

[42] Lee W-K, Nowak RW, Gardella JA. Hydrolytic degradation of polyester blend monolayers at the air/water interface: effects of a slowly degrading component. *Langmuir*. 2002;18(6):2309-2312.

[43] Shukor F, Hassan A, Saiful Islam M, Mokhtar M, Hasan M. Effect of ammonium polyphosphate on flame retardancy, thermal stability and mechanical properties of alkali treated kenaf fiber filled PLA biocomposites. *Materials & Design*. 2014;54:425-429.

[44] Fukushima K, Tabuani D, Abbate C, Arena M, Ferreri L. Effect of sepiolite on the biodegradation of poly(lactic acid) and polycaprolactone. *Polymer Degradation and Stability*. 2010;95(10):2049-2056.

[45] Zaidi L, Kaci M, Bruzard S, Bourmaud A, Grohens Y. Effect of natural weather on the structure and properties of polylactide/Cloisite 30B nanocomposites. *Polymer Degradation and Stability*. 2010;95(9):1751-1758.

[46] Zhang M, Ahmad M, Lee SS, Xu LH, Ok YS. Sorption of Polycyclic Aromatic Hydrocarbons (PAHs) to Lignin: Effects of Hydrophobicity and Temperature. *Bulletin of environmental contamination and toxicology*. 2014;93(1):84-88.

[47] Kudanga T, Prasetyo EN, Sipilä J, Guebitz GM, Nyanhongo GS. Reactivity of long chain alkylamines to lignin moieties: Implications on hydrophobicity of lignocellulose materials. *Journal of biotechnology*. 2010;149(1):81-87.

- [48] Duval A, Molina-Boisseau S, Chirat C. Comparison of Kraft lignin and lignosulfonates addition to wheat gluten-based materials: Mechanical and thermal properties. *Industrial Crops and Products*. 2013;49(0):66-74.
- [49] Kumar R, Yakubu M, Anandjiwala R. Biodegradation of flax fiber reinforced poly lactic acid. 2010.
- [50] Fortunati E, Puglia D, Santulli C, Sarasini F, Kenny J. Biodegradation of Phormium tenax/poly (lactic acid) composites. *Journal of Applied Polymer Science*. 2012;125(S2):E562-E572.
- [51] Fortunati E, Puglia D, Kenny JM, Minhaz-Ul Haque M, Pracella M. Effect of ethylene-co-vinyl acetate-glycidylmethacrylate and cellulose microfibers on the thermal, rheological and biodegradation properties of poly(lactic acid) based systems. *Polymer Degradation and Stability*. 2013(0).
- [52] Gerasimowicz W, Byler D. CARBON-13 CPMAS NMR AND FTIR SPECTROSCOPIC-STUDIES OF HUMIC ACIDS. *Soil science*. 1985;139(3):270-278.
- [53] Kong Y, Hay J. Multiple melting behaviour of poly (ethylene terephthalate). *Polymer*. 2003;44(3):623-633.
- [54] Liu T, Petermann J. Multiple melting behavior in isothermally cold-crystallized isotactic polystyrene. *Polymer*. 2001;42(15):6453-6461.
- [55] Pandey JK, Reddy KR, Kumar AP, Singh R. An overview on the degradability of polymer nanocomposites. *Polymer Degradation and Stability*. 2005;88(2):234-250.
- [56] Fukushima K, Abbate C, Tabuani D, Gennari M, Camino G. Biodegradation of poly(lactic acid) and its nanocomposites. *Polymer Degradation and Stability*. 2009;94(10):1646-1655.
- [57] Yuan X, Mak AF, Yao K. Surface degradation of poly (L-lactic acid) fibres in a concentrated alkaline solution. *Polymer Degradation and Stability*. 2003;79(1):45-52.
- [58] Yussuf A, Massoumi I, Hassan A. Comparison of polylactic acid/kenaf and polylactic acid/rise husk composites: the influence of the natural fibers on the mechanical, thermal and biodegradability properties. *Journal of Polymers and the Environment*. 2010;18(3):422-429.

Table 1: T_g (glass transition), T_{cc} (cold crystallization), T_m (melting) temperatures and crystallinity (X_c) measured in the 1st heating (a) and 2nd heating scans (b) for PLA and PLA/LNP bionanocomposites

(a)

Materials	T_g (°C)	T_{cc} (°C)	T_m (°C)
E-PLA	61.5 ± 0.2	101.7 ± 0.1	170.3 ± 0.3
E-PLA/1LNP	58.6 ± 0.1	100.8 ± 0.1	169.0 ± 0.4
E-PLA/3LNP	60.3 ± 0.3	96.1 ± 0.7	169.3 ± 0.2
C-PLA	46.7 ± 1.5	94.2 ± 0.6	170.1 ± 0.4
C-PLA/1LNP	48.4 ± 0.5	94.9 ± 0.2	170.3 ± 0.3
C-PLA/3LNP	48.3 ± 0.7	95.5 ± 0.2	170.2 ± 0.1

(b)

Materials	T_g (°C)	T_{cc} (°C)	T_m (°C)	X_c (%)
E-PLA	61.5 ± 0.6	100.3 ± 0.8	169.3 ± 0.2	15.0 ± 1.0
E-PLA/1LNP	59.3 ± 0.1	100.3 ± 0.1	168.1 ± 0.3	22.5 ± 1.4
E-PLA/3LNP	60.4 ± 0.1	99.9 ± 0.1	168.9 ± 0.3	17.4 ± 1.1
C-PLA	60.7 ± 0.5	102.6 ± 0.7	169.4 ± 0.4	6.3 ± 0.9
C-PLA/1LNP	60.4 ± 0.1	101.6 ± 0.8	169.2 ± 0.4	7.6 ± 0.3
C-PLA/3LNP	61.4 ± 0.7	101.6 ± 0.8	169.2 ± 0.4	5.5 ± 0.1

Table 2: Onset temperatures, maximum degradation rate temperatures and residual mass at 600°C measured for PLA and PLA/LNP bionanocomposites

Materials	T_{onset(1%)} (°C)	T_{max} (°C)	Residual mass (%) @ 600°C
E-PLA	259.0	351.1	0.02
E-PLA/1LNP	263.7	346.5	1.08
E-PLA/3LNP	274.7	342.8	2.23
C-PLA	290.0	352.6	1.72
C-PLA/1LNP	271.8	351.9	0.33
C-PLA/3LNP	279.6	347.5	0.21

Table 3: Water contact angles for PLA and PLA/LNP bionanocomposites obtained by melting extrusion and solvent casting

Materials	Contact Angle (°)
E-PLA	70.2 ± 2.2
E-PLA/1LNP	71.1 ± 2.0
E-PLA/3LNP	69.8 ± 0.8
C-PLA	50.3 ± 3.1
C-PLA/1LNP	59.1 ± 4.2
C-PLA/3LNP	54.1 ± 3.5

Table 4: T_g (glass transition) and T_m (melting temperatures) measured in the 1st heating scan for PLA and PLA/LNP bionanocomposites at different disintegration times

Materials	T_g ($^{\circ}\text{C}$)			T_m ($^{\circ}\text{C}$)		
	0 days	(3 days (extruded films) (7 days @cast films))	7 days extruded films (15 days cast films)	0 days	(3 days (extruded films) (7 days @cast films))	7 days extruded films (15 days cast films)
E-PLA	60.3	62.8	60.3	170.6	166.4	162.1
E-PLA/1LNP	57.6	62.2	58.2	169.6	166.3	163.9
E-PLA/3LNP	58.2	61.9	58.5	169.5	166.8	162.9
C-PLA	45.1	59.0	48.9	170.2	163.8	145.2
C-PLA/1LNP	48.7	58.7	51.0	170.4	168.3	163.3
C-PLA/3LNP	48.9	61.7	58.2	170.0	168.2	161.1

Figure 1
[Click here to download high resolution image](#)

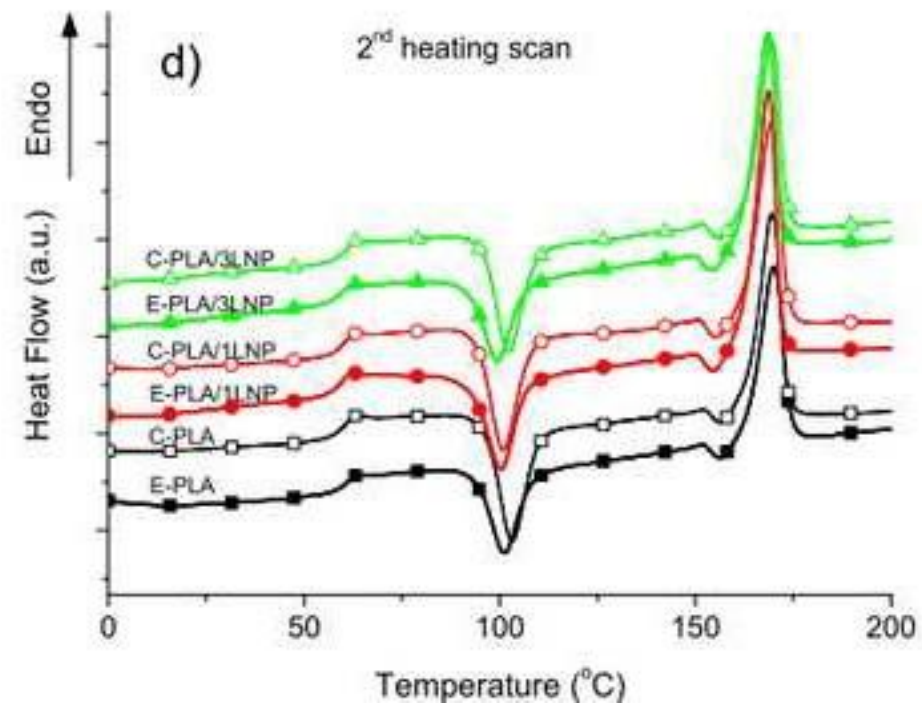
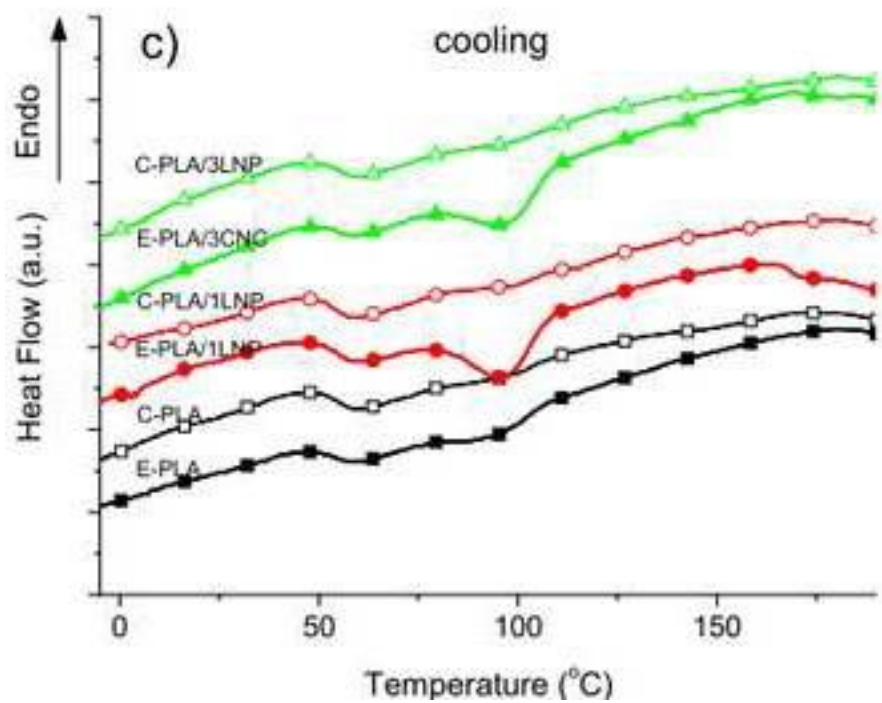
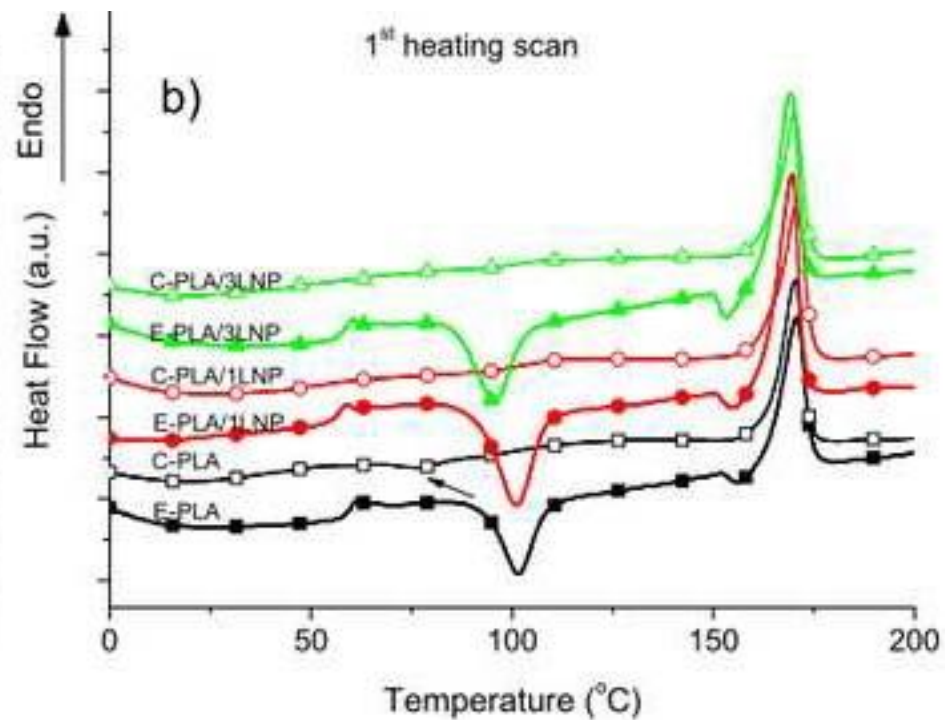
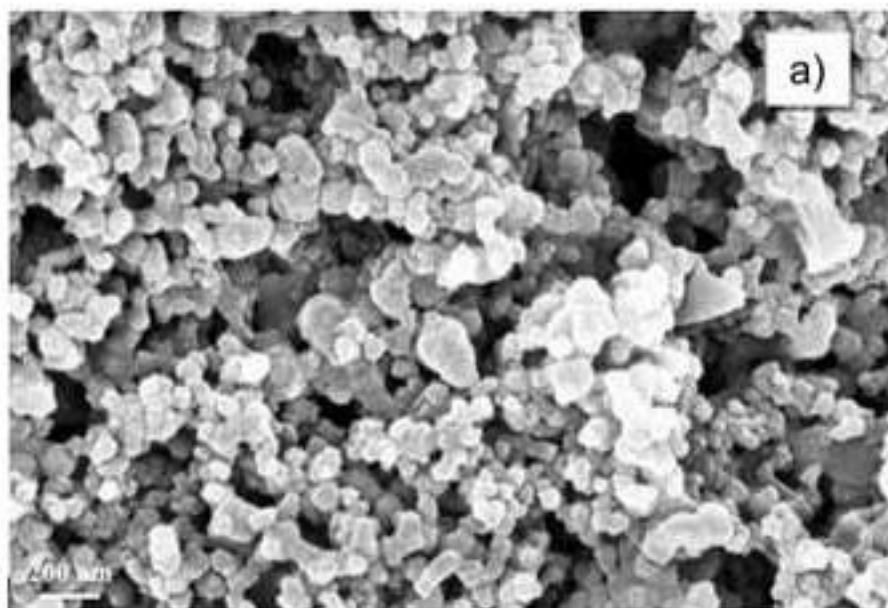


Figure 2
[Click here to download high resolution image](#)

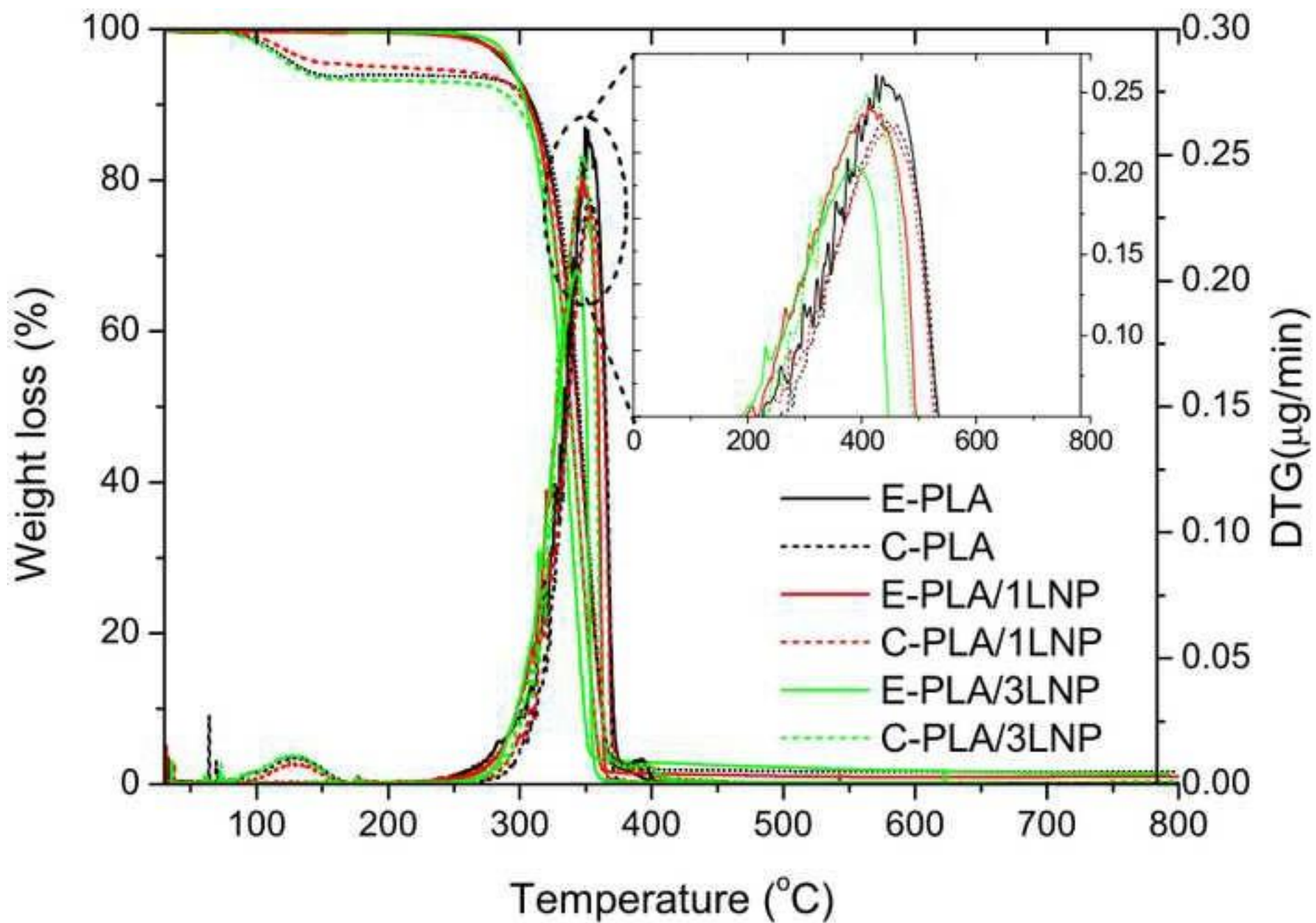


Figure 3
Click here to download high resolution image

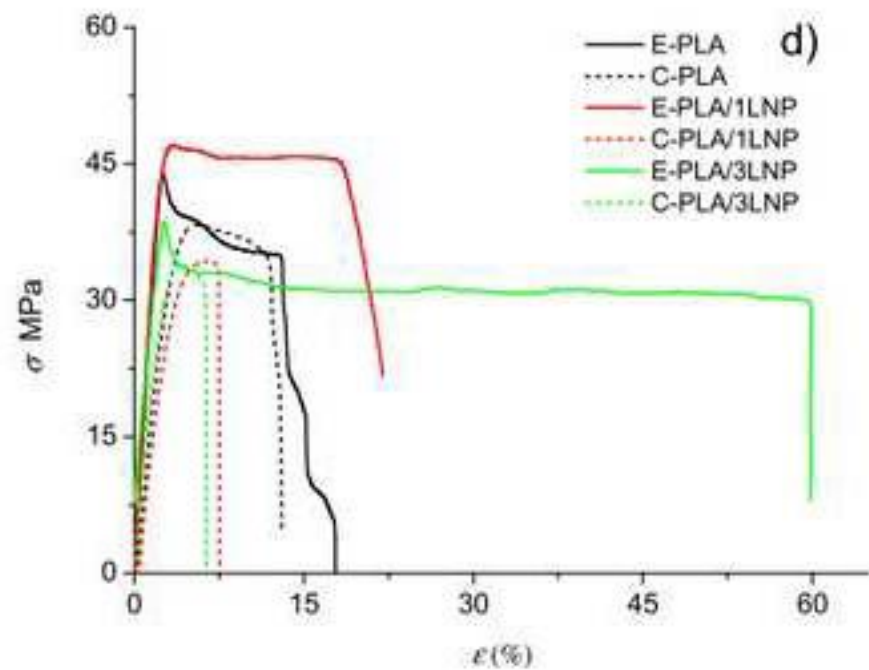
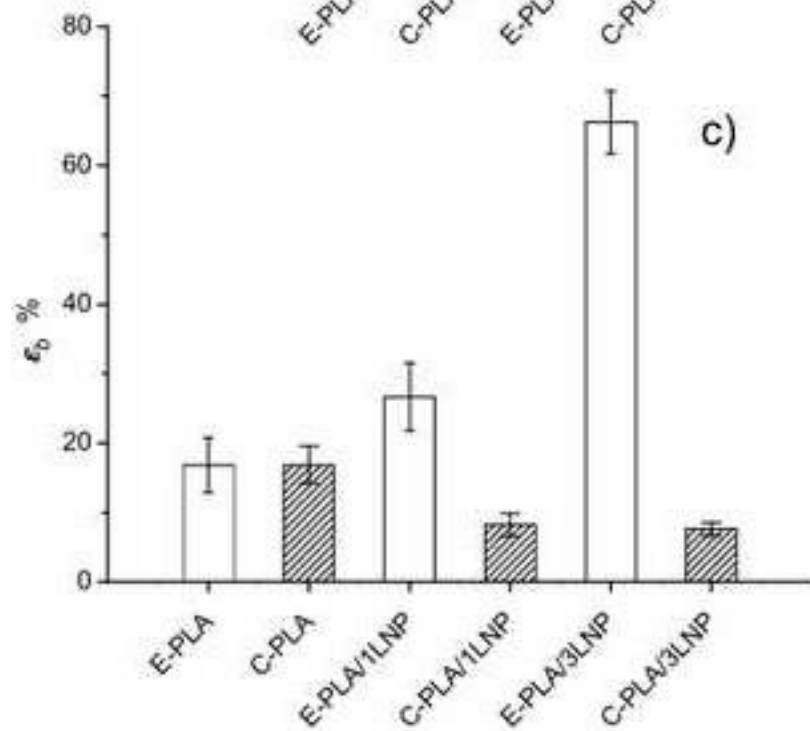
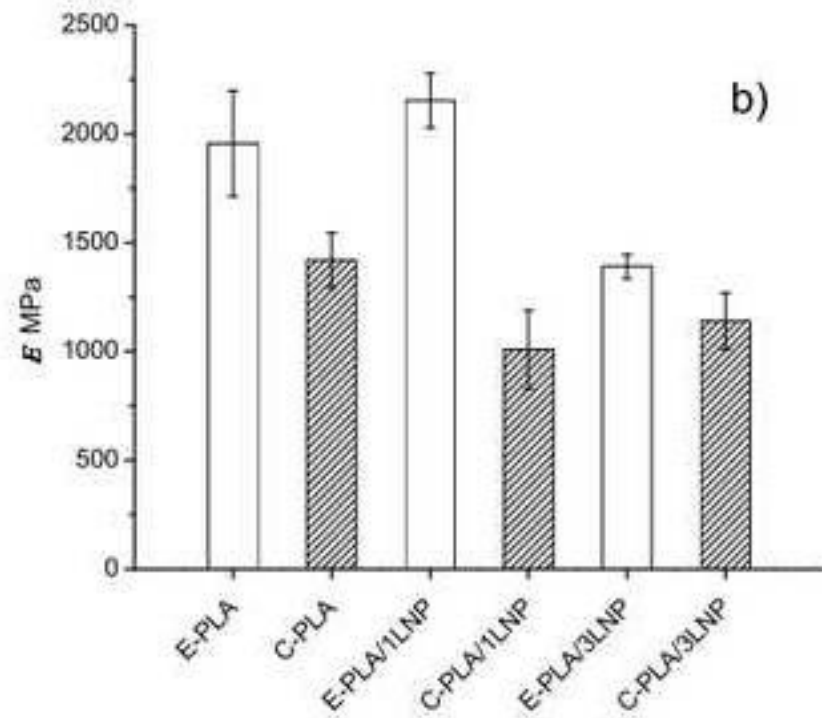
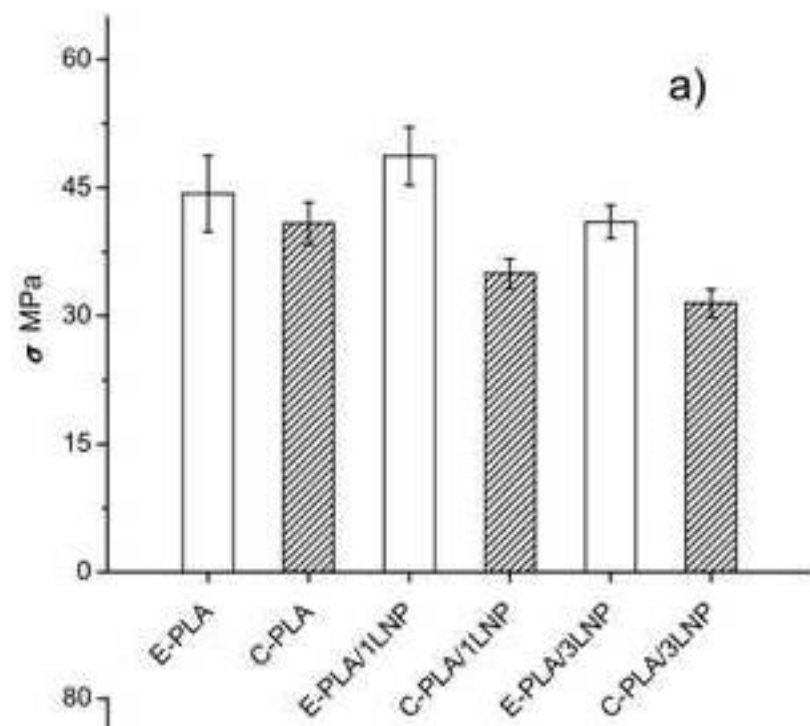


Figure 4
[Click here to download high resolution image](#)

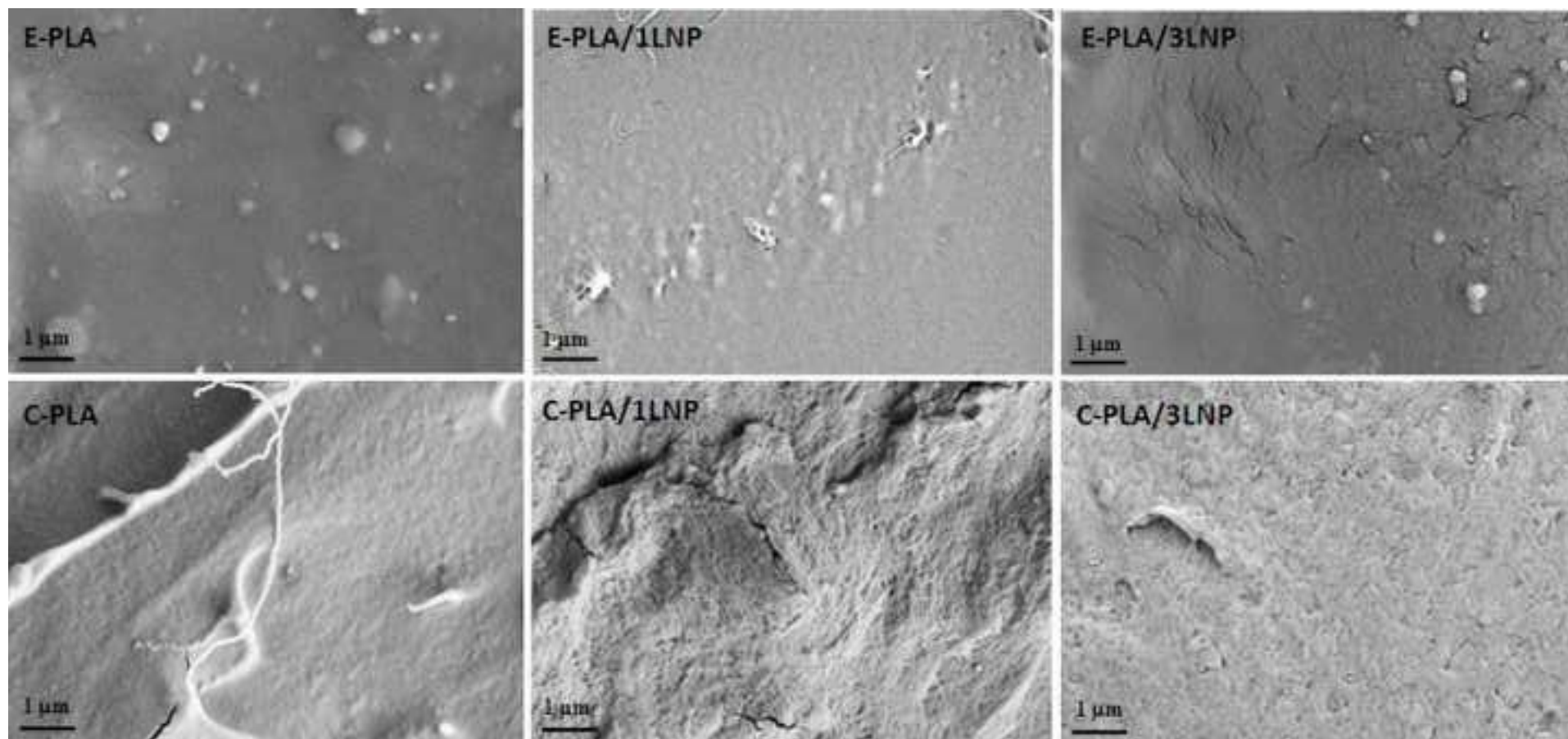


Figure 5a
[Click here to download high resolution image](#)



















Measurement time	0 days	1 Day	3 Days	7 Days	10 Days	15 Days
E-PLA						
E-PLA/1LNP						
E-PLA/3LNP						

Figure 5b
[Click here to download high resolution image](#)

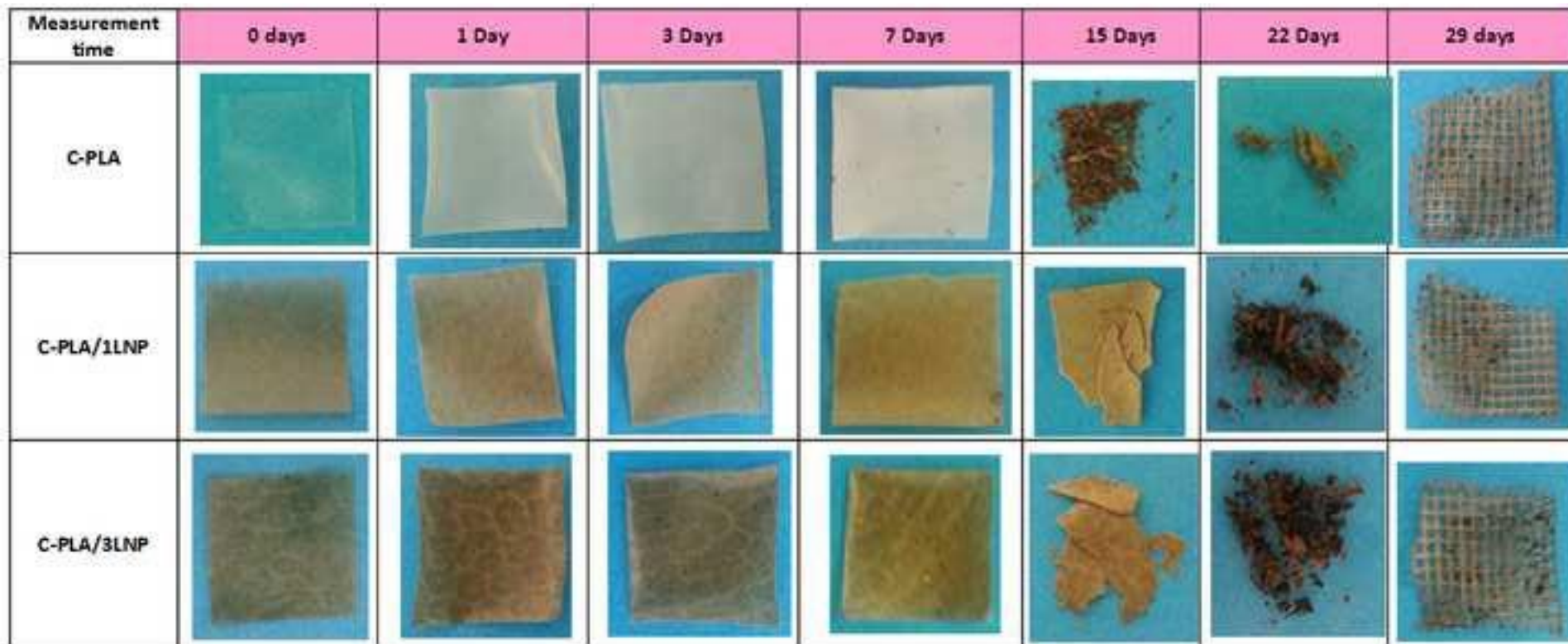


Figure 6
[Click here to download high resolution image](#)

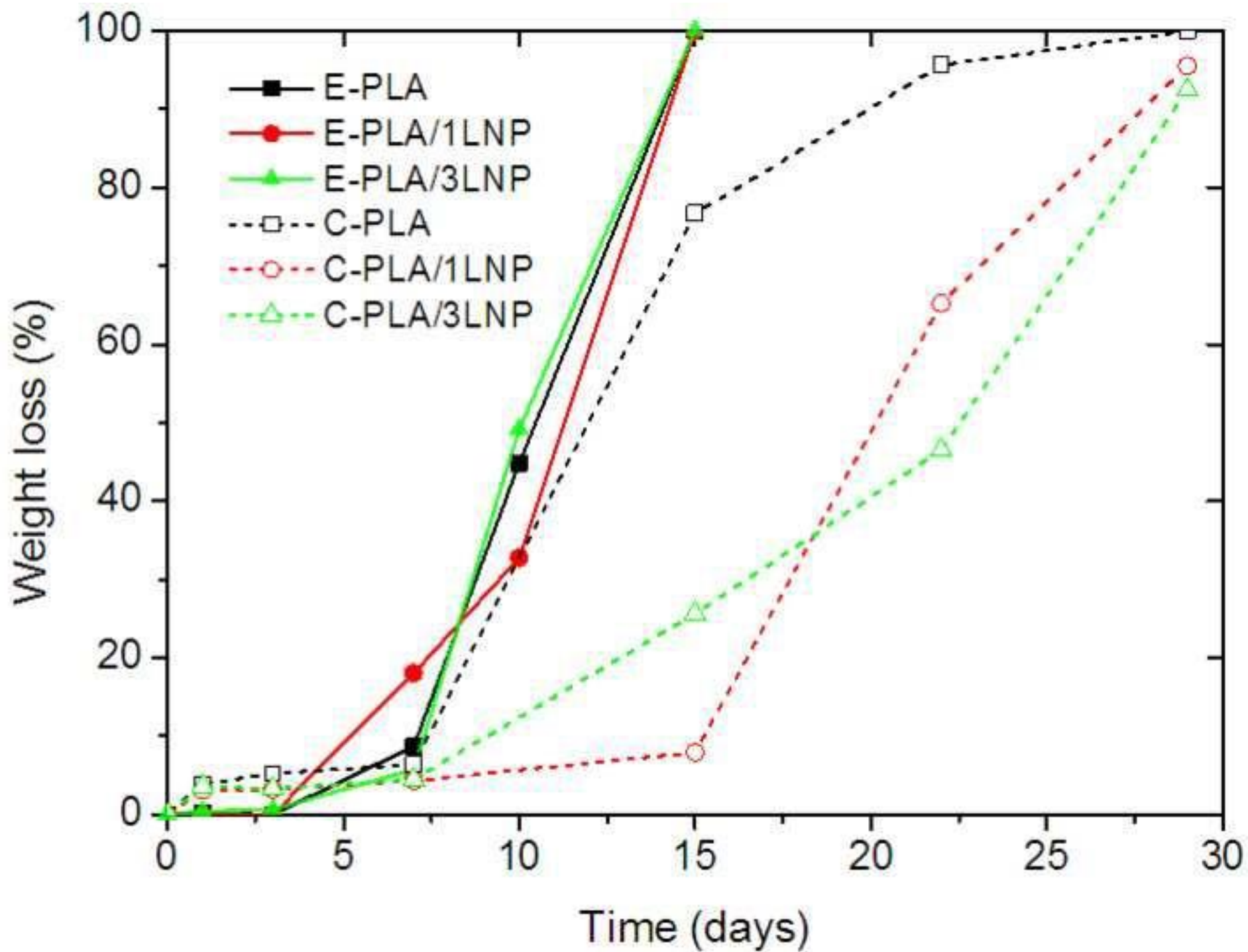


Figure 7
[Click here to download high resolution image](#)

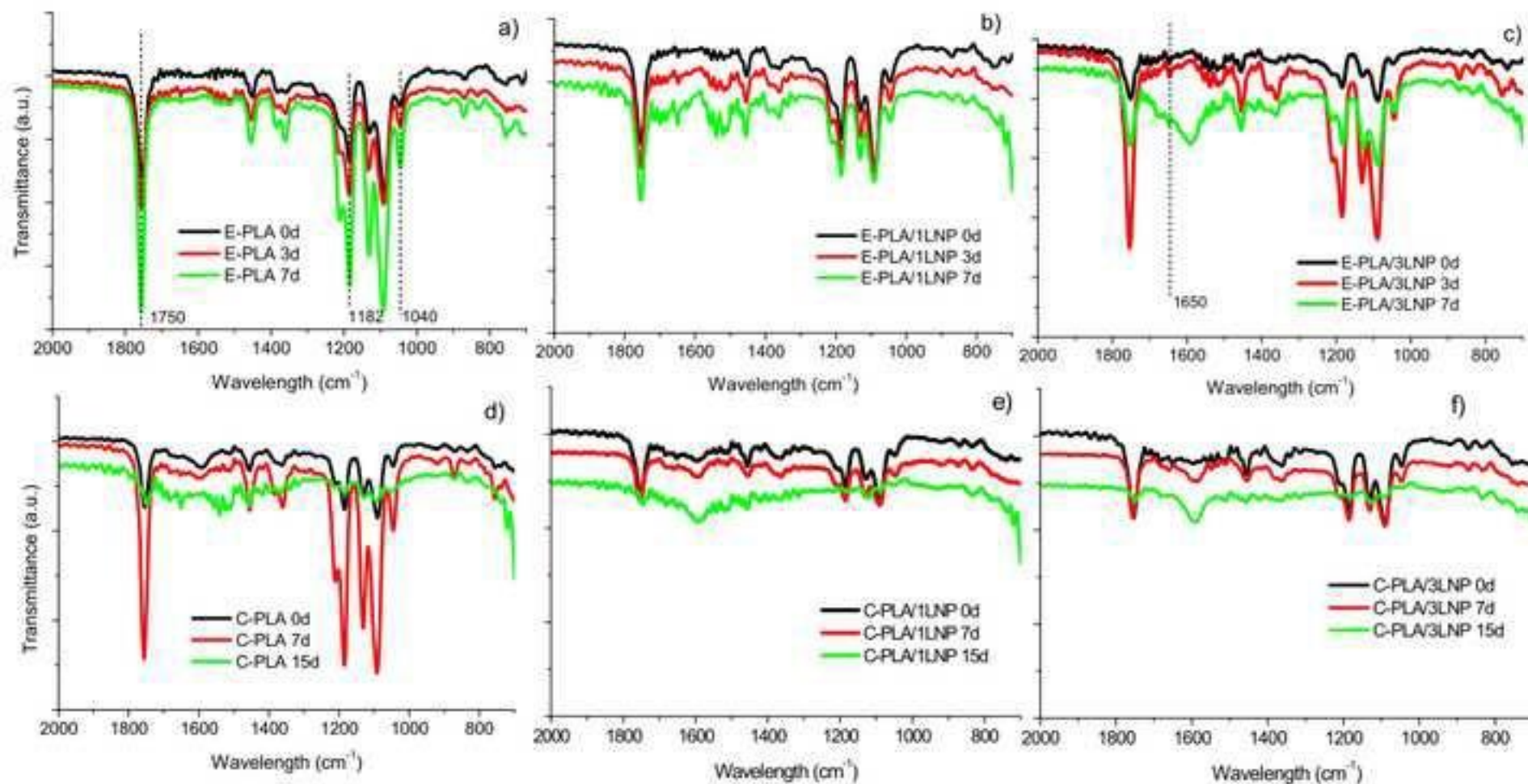


Figure 8
Click here to download high resolution image

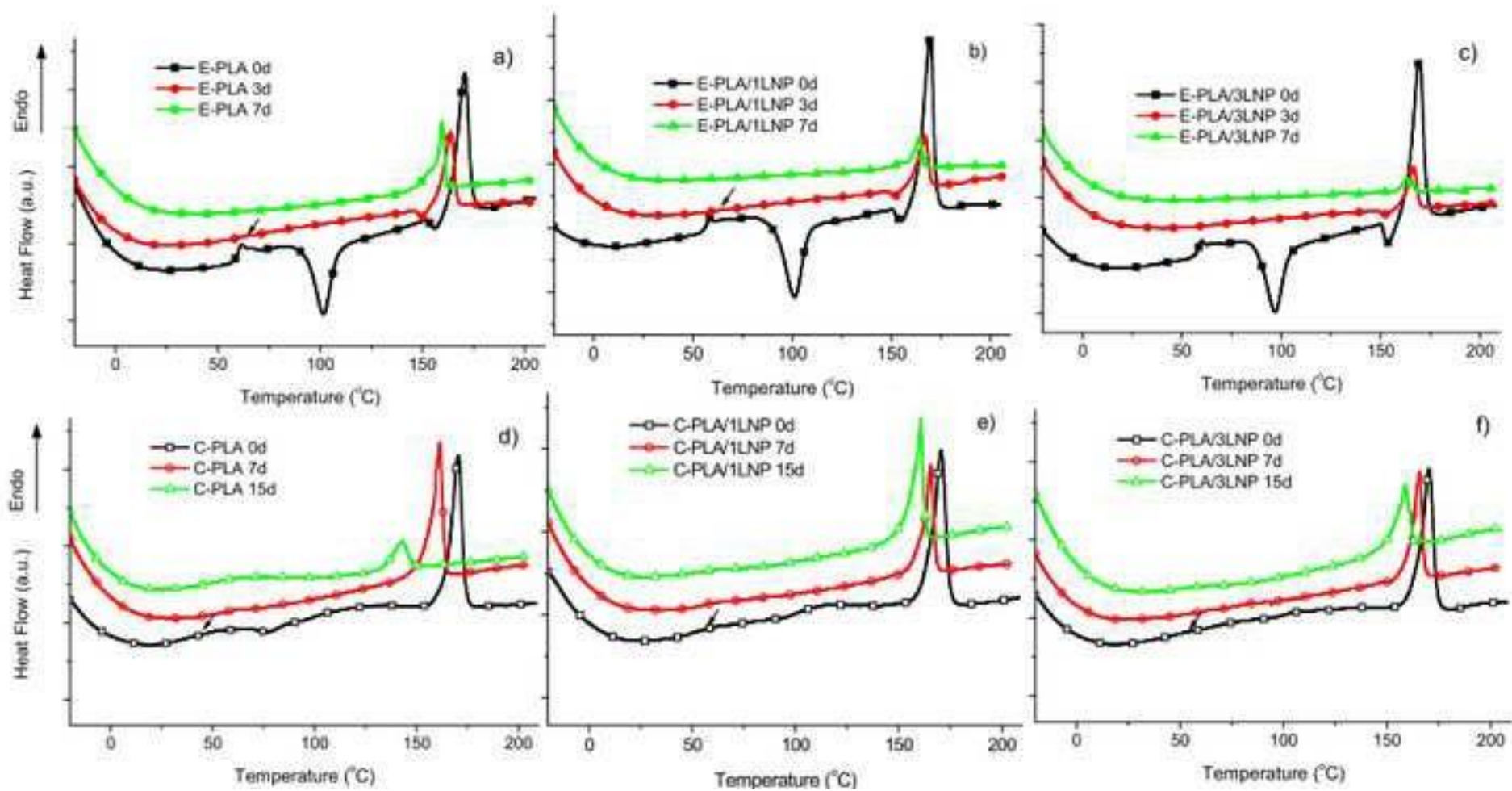


Figure 9a
[Click here to download high resolution image](#)

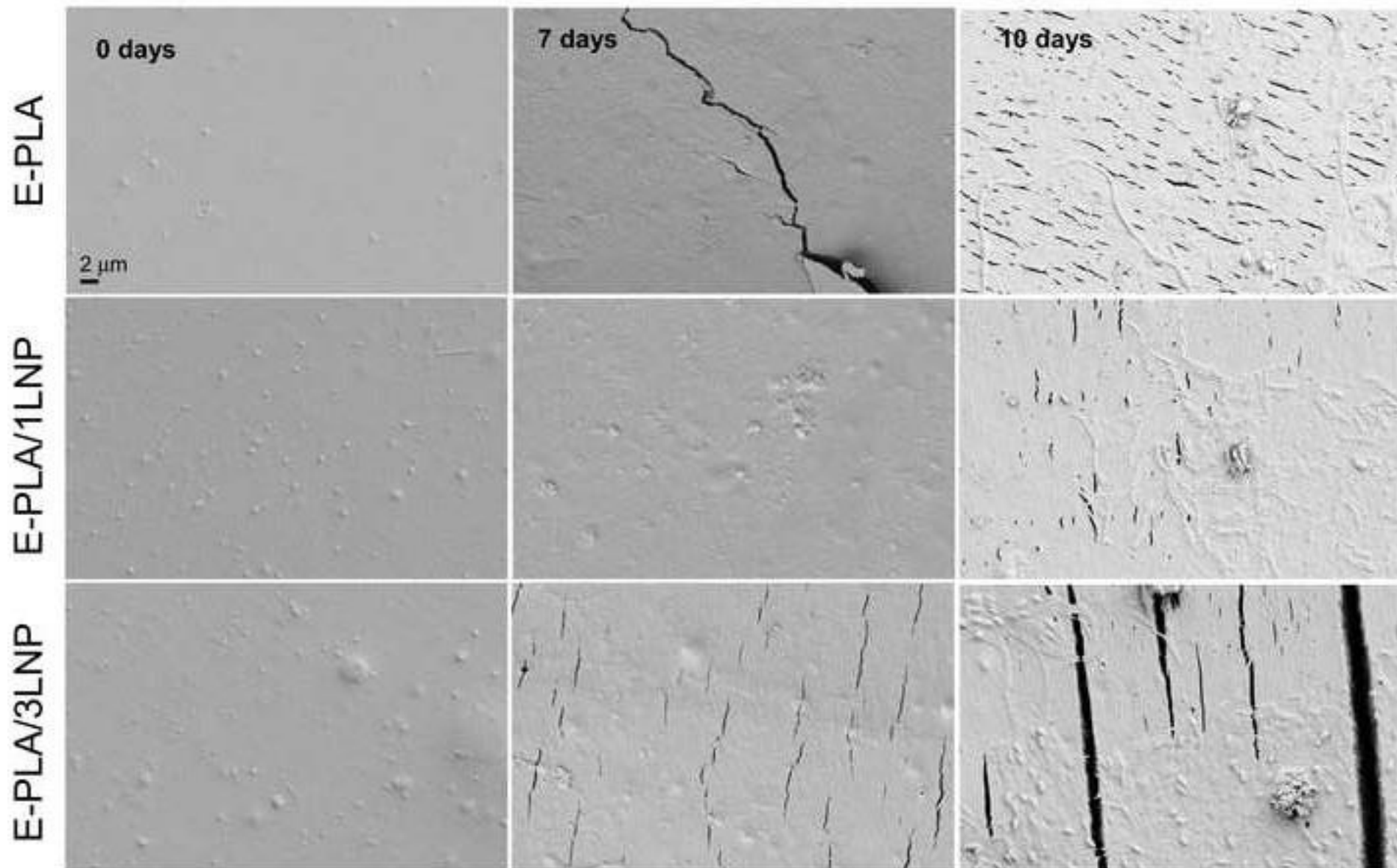


Figure 9b
[Click here to download high resolution image](#)

